Determining the finite difference weights for the acoustic wave equation by a new dispersion-relationship-preserving method

Wenquan Liang Yanfei Wang* and Changchun Yang

Key Laboratory of Petroleum Resources Research,

Institute of Geology and Geophysics,

Chinese Academy of Sciences,

P.O.Box 9825, Beijing, 100029, P.R.China

In original form 2012 December 27

Abstract

Numerical simulation of the acoustic wave equation is widely used to theoretically synthesize seismograms, and constitutes the basis of the reverse time migration. With finite difference methods, the discretization of the temporal and spatial derivatives in the wave equations introduces numerical grid dispersion. To reduce the grid dispersion effect, we propose to satisfy the dispersion relation for a number of uniformly distributed wavenumber points within a wavenumber domain with the upper limit determined by the maximum source frequency, the grid spacing and the wave velocity. This new dispersion relationship preserving method relatively uniformly reduces the numerical dispersion over a large frequency range. Dispersion analysis and seismic numerical simulations demonstrate the effectiveness of the proposed method.

Key words: Acoustic wave equation modeling, Finite difference weights, dispersion relation preserving

*E-mail: yfwang@mail.iggcas.ac.cn

1 Introduction

The propagation of the seismic waves through the earth subsurface is described by the wave equation, one of the partial differential equations (PDEs), which describe many of the fundamental natural laws. Seismic wave equation simulations constitute the basis for the reverse time migration and the full waveform inversion. Finite difference (FD) methods are usually preferred over other numerical methods for seismic modeling, and the need for higher order finite difference operators has long been recognized (Kelley et al., 1976; Dablain, 1986). The FD methods are efficient in calculation since the methods need less memory and are easy to be implemented, hence are widely used in seismic forward problems and reverse time migration (Bansal and Sen, 2008; Buur and T. Kuhnel, 2008; Etgen and O'Brien, 2007; Guan et al., 2011; McMechan, 1989; Yang et al., 2012; Zhang et al., 2011). And also recent works show that this method can be greatly accelerated using graphics processing unit clusters (Abdelkhalek et al., 2012; Liu et al., 2012). A review of applications of the FD methods to geophysical imaging is given in (Virieux et al., 2011).

Grid dispersion is one of the key numerical problems affecting the practical usage when utilizing the finite difference method. The dispersion is due to the gridding in spatial and temporal partial derivatives of the acoustic wave equation. After discretization, the phase velocity becomes the function of the grid intervals, which may cause the numerical phase velocity to be unequal to the true velocity of earth medium, and hence reduce the precision of seismic wave simulations. Generally speaking, a finite difference scheme dominated by spatial dispersion decreases the phase velocities of high frequencies, while a finite difference scheme dominated by temporal dispersion increases the phase velocities of high frequencies (Dablain, 1986). To reduce or suppress the grid dispersion, two techniques are usually adopted. The first technique is the adoption of the lower order FD scheme, which requires sufficiently small temporal and spatial grid steps, however this may cause large storage of data and huge computational costs. The other technique utilizes the higher order FD scheme, e.g., second order derivatives in the temporal direction and higher order FD scheme in the spatial direction.

Previous methods for determining the FD coefficients using the higher-order FD scheme through Taylor expansion can preserve dispersion property only in limited frequency range and angle domain. Ye and Chu (2005) proposed a dispersion-relationship-preserving method which could preserve dispersion property in a

large frequency range. Fornberg (1987) proved that the pseudospectral method can be interpreted as the limit of finite difference schemes with increasing orders. Recently, Chu and Stoffa (2012) improved the finite difference methods thanks to a scaled binomial windowed FD scheme that leads to more precise discrete operators. However, these methods did not consider the source frequency spectrum, the spatial grid interval and the velocity variations when calculating the FD coefficients. In this paper, we pay attention to the maximum of the source frequency, the spatial grid interval and the variations of the velocity when calculating the FD coefficients. Through dispersion analysis and numerical simulations, we conclude that the new method is applicable in seismic wave modeling.

2 Previous Methods for Determining the FD Coefficients in Spatial Space

Assume that the function $f(x)$ is twice differentiable. The first-order derivative of the function $f(x)$ could be approximated by a $2N$-order FD operator (Chu and Stoffa, 2012)

$$\frac{\partial f}{\partial x} = \frac{1}{\Delta x}\sum_{n=1}^{N} c_n(f_n - f_{-n}), \tag{1}$$

where $f_n = f(x+n\Delta x)$, Δx is the grid interval in x direction and c_n for all n are FD coefficients.

Taking Fourier transform of both sides of (1) and differentiating it with respect to x, according to equation (1), we obtain

$$k_x\Delta x = 2\sum_{n=1}^{N} c_n \sin(nk_x\Delta x), \tag{2}$$

where k_x is the wavenumber. The FD coefficients are determined by finding the Taylor expansion of the sine function in (2) and then matching the term $k_x\Delta x$.

Similarly, the second-order derivative of the function $f(x)$ could be approximated by a $2N$-order FD operator

$$\frac{\partial^2 f}{\partial x^2} = \frac{1}{\Delta x^2}[c_0 f_0 + \sum_{n=1}^{N} c_n(f_{-n} + f_n)] \tag{3}$$

where c_n for all n are FD coefficients.

Applying Fourier transform to $f(x)$ and taking second-order derivatives to x, according to equation (3), we

obtain

$$-(k_x\Delta x)^2 = c_0 + 2\sum_{n=1}^{N} c_n \cos(nk_x\Delta x) \tag{4}$$

where k_x is again referred as the wavenumber.

Similarly, taking Taylor expansion of the cosine function in (4) and matching the term $k_x\Delta x$, the FD coefficients of the second-order derivative of the function $f(x)$ could be obtained. However, with these classical FD coefficients, the error between the exact and the discrete dispersion relation increases significantly with frequencies. Therefore, Ye and Chu (2005) improved the numerical scheme by proposing a new dispersion relationship preserving method.

The FD method can be interpreted as a binomial window truncated convolutional counterpart of the pseudospectral method in the space domain, i.e., the coefficients satisfy (Chu and Stoffa ,2012)

$$c_n = -\frac{2}{n^2}\cos(n\pi)w_n^{2N}, n = \pm1, \pm2, \cdots, \pm N, \tag{5}$$

$$c_0 = -\sum_{n=1}^{N}(c_{-n} + c_n), \tag{6}$$

where $w_n^{2N} = \frac{C_{2N}^{N+n}}{C_{2N}^{N}}$ is a window-weighting coefficient, $C_m^l = \frac{m!}{l!(m-l)!}$ and $m \geq l$. They also proposed a optimized binomial window to enhance dispersion properties, i.e., the window-weighting coefficient w_n^{2N} was changed to w_n^{2N+M} and the FD coefficients satisfy

$$c_n = -\frac{2}{n^2}(\cos n\pi)w_n^{2N+M}, n = \pm1, \pm2, \cdots, \pm N, \tag{7}$$

where M is a nonnegative even number which restricts the FD operator to a specified wavenumber range. However the method requires adjusting the size of the window properly, which is a delicate thing.

3 New Methods for Determining the FD Coefficients

3.1 Dispersion-relationship-preserving FD operators: first derivative in 1D case

For previous methods, they do not give an accurate wavenumber range which is required before optimizing the FD coefficients. However, an accurate wavenumber range is important for optimization. If the wavenumber range is too small, the optimization method degenerates to the Taylor expansion method. On the contrary, if

the wavenumber range is too large, the dispersion error in low frequencies will be obvious. In our approach, we select a set of given wavenumbers within a proper wavenumber range and equates the discretized dispersion relation to the exact dispersion relation at those points. In our approach, we determine the wavenumber range by

$$r = \frac{k_u \Delta x}{\pi} = \frac{f}{v/2\Delta x}, \tag{8}$$

where f is related to the maximum frequency of the source, v is the velocity, k_u is the upper limit of the wavenumber used for computing the FD coefficients and Δx is the spatial grid interval. For example, when the maximum source frequency is 40Hz, the velocity 2000m/s and the grid spacing 20m, $k_u \Delta x$ equals 80% times π; if the maximum frequency of the source is 30Hz, then $k_u \Delta x$ becomes 60% times π. This definition is related to the Nyquist criterium. We notice that the Nyquist criterion corresponds to $r = 1$, leading to two points per wavelength. However, this theoretical limit is not usable in practice with finite difference scheme. We therefore impose an upper bound on the wavenumbers.

Remark 1 *With our approach, if we consider a too high upper limit for the wavenumber for a given scheme order and grid spacing, large numerical dispersion will appear at low frequencies; while if we consider a too small upper limit for the wavenumber, large numerical dispersion will appear at high frequencies. Percentage of $k_u \Delta x$ to π is given by $f/(v/(2\Delta x))$.*

We assume that there are N grid points satisfying the dispersion property within the wavenumber determined by the above method. Then we can establish the following equations:

$$\begin{bmatrix} 2\sin(k_x(1)\Delta x) & 2\sin(2k_x(1)\Delta x) & \cdots & 2\sin(Nk_x(1)\Delta x) \\ \vdots & \vdots & \vdots & \vdots \\ 2\sin(k_x(N)\Delta x) & 2\sin(2k_x(N)\Delta x) & \cdots & 2\sin(Nk_x(N)\Delta x) \end{bmatrix} \begin{bmatrix} c_1 \\ \vdots \\ c_N \end{bmatrix} = \begin{bmatrix} k_x(1)\Delta x \\ \vdots \\ k_x(N)\Delta x \end{bmatrix}, \tag{9}$$

where $k_x(n)\Delta x$ ($n = 1, 2, \cdots, N$) are equally distributed between $r\pi/N$ and $r\pi$. The condition number of the matrix of above equations is less than that from the traditional method, hence it is easy to solve for the FD coefficients.

3.2 Dispersion-relationship-preserving FD operators: second derivative in 1D case

For the FD operator of the second derivative, we again determine the upper limit of the wavenumber based on the source frequency, the grid interval and the wave velocity. We assume that there are $N+1$ grid points satisfying the dispersion property within the wavenumber specified by (8). Then we can establish the following equations:

$$\begin{bmatrix} 1 & 2\cos(k_x(1)\Delta x) & \cdots & 2\cos(Nk_x(1)\Delta x) \\ \vdots & \vdots & \vdots & \vdots \\ 1 & 2\cos(k_x(N)\Delta x) & \cdots & 2\cos(Nk_x(N)\Delta x) \end{bmatrix} \begin{bmatrix} c_0 \\ \vdots \\ c_N \end{bmatrix} = \begin{bmatrix} -[k_x(1)\Delta x]^2 \\ \vdots \\ -[k_x(N+1)\Delta x]^2 \end{bmatrix}. \tag{10}$$

For the linear equations, either direct decomposition methods or iterative solvers can be applied for finding the FD coefficients.

3.3 Dispersion-relationship-preserving FD operators of the two-dimensional acoustic wave equation

The acoustic wave equation in 2D can be written as

$$\frac{\partial^2 p}{\partial x^2} + \frac{\partial^2 p}{\partial z^2} = \frac{1}{v^2}\frac{\partial^2 p}{\partial t^2}, \tag{11}$$

where $p = p(x,z,t)$ represents the wavefield. Utilizing the same coefficients in the x and z directions, we obtain the following FD scheme

$$\begin{cases} \frac{\partial^2 p}{\partial x^2} \approx \frac{\delta^2 p}{\delta x^2} = \frac{1}{h^2}(c_0 p^0_{0,0} + \sum_{m=1}^{N} c_m (p^0_{-m,0} + p^0_{m,0})), \\ \frac{\partial^2 p}{\partial z^2} \approx \frac{\delta^2 p}{\delta z^2} = \frac{1}{h^2}(c_0 p^0_{0,0} + \sum_{m=1}^{N} c_m (p^0_{0,-m} + p^0_{0,m})), \end{cases} \tag{12}$$

where $p^j_{m,n} = p(x+mh, z+nh, t+j\tau)$, h denotes the grid spacing (we assume the same grid step size in x and z directions), τ denotes the time step and N is the length of the FD operator.

Applying Fourier transform to (12), we obtain

$$-k^2h^2 \approx 2c_0 + \sum_{m=1}^{N} 2c_m(\cos(mkh\sin\theta) + \cos(mkh\cos\theta)). \tag{13}$$

For the FD operator of the second order derivative, we again determine the upper limit of the wavenumber based on the source frequency, the grid interval and the wave velocity. We assume that there are $N+1$ grid points satisfying the dispersion property within the wavenumber specified by (13). Then we can establish the following equations:

$$\sum_{\theta=0}^{2\pi}\begin{bmatrix} 1 & a^h_{k_{1,l},1} & \cdots & a^h_{k_{1,l},N} \\ \vdots & \vdots & \vdots & \vdots \\ 1 & a^h_{k_{N+1,l},1} & \cdots & a^h_{k_{N+1,l},M} \end{bmatrix}\begin{bmatrix} c_0 \\ \vdots \\ c_N \end{bmatrix} = \frac{1}{2}\sum_{\theta=0}^{2\pi}\begin{bmatrix} -k(1)^2h^2 \\ \vdots \\ -k(N+1)^2h^2 \end{bmatrix}, \tag{14}$$

where we define $a^h_{k_l,m}$=$\cos(mk_xh)+\cos(mk_zh)$ $(m=1,\cdots,N)$, $k_{i,l}$ $(i=1,\cdots,N+1)$ is the i-th component of k_l $(l=x,z)$, $k_x=k\cos\theta$, $k_z=k\sin\theta$, and θ is the propagation angle of the plane wave ($\theta=\frac{j}{4}\pi$, $j=0,1,\cdots,8$).

For the linear equations, either direct decomposition methods or iterative solvers can be applied for finding the FD coefficients.

3.4 Dispersion-relationship-preserving FD operators of the three-dimensional acoustic wave equation

Now, we consider the acoustic wave equation in 3D,

$$\frac{\partial^2 p}{\partial x^2}+\frac{\partial^2 p}{\partial y^2}+\frac{\partial^2 p}{\partial z^2}=\frac{1}{v^2}\frac{\partial^2 p}{\partial t^2}, \tag{15}$$

where $p=p(x,y,z,t)$ represents the wavefield. Utilizing the same coefficients for x, y and z directions, we have the following difference scheme

$$\begin{cases} \frac{\partial^2 p}{\partial x^2}\approx\frac{\delta^2 p}{\delta x^2}=\frac{1}{h^2}(c_0p^0_{0,0,0}+\sum\limits_{m=1}^{N}c_m(p^0_{-m,0,0}+p^0_{m,0,0})), \\ \frac{\partial^2 p}{\partial y^2}\approx\frac{\delta^2 p}{\delta y^2}=\frac{1}{h^2}(c_0p^0_{0,0,0}+\sum\limits_{m=1}^{N}c_m(p^0_{0,-m,0}+p^0_{0,m,0})), \\ \frac{\partial^2 p}{\partial z^2}\approx\frac{\delta^2 p}{\delta z^2}=\frac{1}{h^2}(c_0p^0_{0,0,0}+\sum\limits_{m=1}^{N}c_m(p^0_{0,0,-m}+p^0_{0,0,m})), \end{cases} \tag{16}$$

where c_i for all i are FD coefficients, $p^j_{m,n,l}=p(x+mh,y+nh,z+lh,t+j\tau)$, h is the spatial grid step size (we assume the same grid step size in all spatial directions), τ is the temporal step size and m is the length of the FD operator.

Taking the Fourier transform of both sides of equation (16), we obtain

$$-k^2h^2 \approx 3c_0 + 2\sum_{m=1}^{N} c_m(\cos(mkh\cos\theta\cos\phi) + \cos(mkh\cos\theta\sin\phi) + \cos(mkh\sin\theta)), \tag{17}$$

where k denotes the wavenumber satisfying $k = \sqrt{k_x^2 + k_y^2 + k_z^2}$, θ is the plane wave propagation angle to the surface and ϕ is the azimuth of the plane wave.

For the FD operator of the second order derivative, we again determine the upper limit of the wavenumber based on the source frequency, the spatial grid interval and the wave velocity. We assume that there are $N+1$ grid points satisfying the dispersion property within the wavenumber, and define

$$a^h_{k_l,m} = \cos(mk_xh) + \cos(mk_yh) + \cos(mk_zh), \quad (m = 1, \cdots, N)$$

where the i-th component of k_l $(l = x, y, z)$ is denoted by $k_{i,l}$ $(i = 1, \cdots, N+1)$, $k_x = k\cos\theta\cos\phi$, $k_y = k\cos\theta\sin\phi$, $k_z = k\sin\theta$, and the plane wave propagation angle θ and the azimuth of the plane wave ϕ satisfying $\theta, \phi = \frac{j}{4}\pi$, $j = 0, 1, \cdots, 8$. Noticing equation (17), we obtain the following equations:

$$\sum_{\phi=0}^{2\pi}\sum_{\theta=0}^{2\pi} \begin{bmatrix} 3/2 & a^h_{k_{1,l},1} & \cdots & a^h_{k_{1,l},N} \\ \vdots & \vdots & \vdots & \vdots \\ 3/2 & a^h_{k_{N+1,l},1} & \cdots & a^h_{k_{N+1,l},N} \end{bmatrix} \begin{bmatrix} c_0 \\ \vdots \\ c_N \end{bmatrix} = \frac{1}{2}\sum_{\phi=0}^{2\pi}\sum_{\theta=0}^{2\pi} \begin{bmatrix} -k(1)^2h^2 \\ \vdots \\ -k(N+1)^2h^2 \end{bmatrix}. \tag{18}$$

This is a linear system in $N+1$ unknowns. So again direct decomposition methods or iterative solvers can be applied for computing the FD coefficients.

3.5 Solving the linear equations

Now we consider the computational issues of the systems of linear algebraic equations for retrieving the FD coefficients. From equations (9), (10), (14) and (18), the linear equations for determining the FD coefficients can be written as

$$Ax = b, \tag{19}$$

where $A \in \mathbb{R}^{(N+1)\times(N+1)}$, x denotes the FD coefficients and $b \in \mathbb{R}^{(N+1)\times 1}$. Now the remaining task is solving the linear equations to give the coefficients x. In our numerical tests, a Gaussian elimination method is performed.

We report that the condition number of the matrix A to define the stencil coefficients with our new method is smaller than the one of the traditional method. For the traditional method, according to the Taylor expansion of the equation (4), if we calculate the condition number of the corresponding matrix A, the results are: cond(A) can be up to $O(10^{20})$ for calculating the FD coefficients when $N = 10$; for $N = 20$, cond(A) can be up to 10^{52}. This clearly means that the solution of the above linear equation for the FD coefficients is unstable, and it may bring a wrong interpretation. Using our dispersion-relationship-preserving FD operator, the results are: cond(A) is in the magnitude of $O(10^3)$ for $N = 10$; while for $N = 20$, cond(A) is in the magnitude of $O(10^8)$. The condition numbers are much smaller than that of the traditional method. Therefore, we may conclude that the FD coefficients calculated using our method are more reliable.

4 Numerical dispersion error analysis

We will now compare the numerical dispersion errors in different cases. First, we use the following formulae

$$E_1^1 = 2\sum_{n=1}^{N} c_n \sin(nk_x\Delta x) - k_x\Delta x \tag{20}$$

and

$$E_1^2 = -[c_0 + 2\sum_{n=1}^{N} c_n \cos(nk_x\Delta x)] - (k_x\Delta x)^2 \tag{21}$$

to measure the dispersion errors of the FD operator for the first and second derivatives, respectively. The smaller values of E_1^1 and E_1^2, the less dispersion of the 1D FD operator will be.

Comparison of the dispersion errors of the FD operator using traditional FD scheme, Chu and Stoffa's FD scheme and our new FD scheme for the first derivative, is shown in Figure 1. The values of r of the proposed method in Figure 1 are 0.59, 0.64, 0.8, 0.85 and 0.89 for different values of the number N, respectively. It indicates from Figures 1(a) and 1(b) that to maintain the dispersion error to be less than 1.0×10^{-4} and cover the similar kh range ($[0, 0.6\pi]$), the traditional method requires a 41-point FD operator, whereas the new method needs a 17-point FD operator. With increase of the length of the FD operator, the kh range of the traditional method increases slowly, while the new method can preserve the dispersion relation in a larger kh range. Figures 1(c) and 1(d) show the comparison results of the new method with the method of Chu and Stoffa

(2012). To maintain the dispersion error to be less than 10^{-4} and keep the similar kh range ($[0, 0.6\pi]$), the new method needs a shorter FD operator than that of (Chu and Stoffa, 2012). Moreover, our new dispersion-relationship-preserving method can preserve the dispersion relation within a larger kh range. As it is shown in Figures 1(c) and 1(d) that, a 81-point FD operator with the new method can cover 90% of kh range under the error limitation 0.0001. In (Zhang et al., 2011) (see Figure 1 in their paper), their first-order method could maintain the numerical dispersion at high Nyquist wavenumbers (80%-92%), however, their method requires an extremely high-order FD scheme, which may cost a lot of computation; while our method could maintain similar dispersion relation using low-order FD scheme. In the method of (Chu and Stoffa, 2012), as $2N > 60$, the dispersion errors do not decrease with increase of the length of the FD operator.

Comparison of the dispersion errors of the FD operator using the traditional FD scheme, Chu and Stoffa's FD scheme and our new FD scheme for the second derivative, is shown in Figure 2. Similar results could be achieved that the new method needs shorter FD operator to maintain the dispersion relation than the traditional method and the method of (Chu and Stoffa, 2012). Note that the longer the FD operator, the more ill-conditioned the linear system (19) will be. Hence the FD coefficients calculated using our new method are more reliable.

We use the following formula to measure the dispersion errors of the 2D FD operator for the second derivative:

$$E_2 = -[2c_0 + 2\sum_{n=1}^{N} c_n \cos(nk\cos(\theta)h) + 2\sum_{n=1}^{N} c_n \cos(nk\sin(\theta)h)] - (kh)^2. \tag{22}$$

The smaller value of E_2, the less dispersion of the 2D FD operator will be.

Below we present several comparison results on dispersion errors of the 2D case. The dispersion error of the traditional FD operator when $N = 8$ is shown in Figure 3(a). With the same length of the FD operator, the dispersion error of the optimized binomial windowed method (see equation (7)) is displayed in Figure 3(b), while the dispersion error of the new dispersion-relationship-preserving method is illustrated in Figure 3(c). To clearly show the dispersion effect, we zoomed Figures 3(a)-3(c) to Figures 4(a)-4(c), respectively. It is obvious that the new method can preserve dispersion relation within a larger interval of frequencies and angles. The results agree with the 1D case.

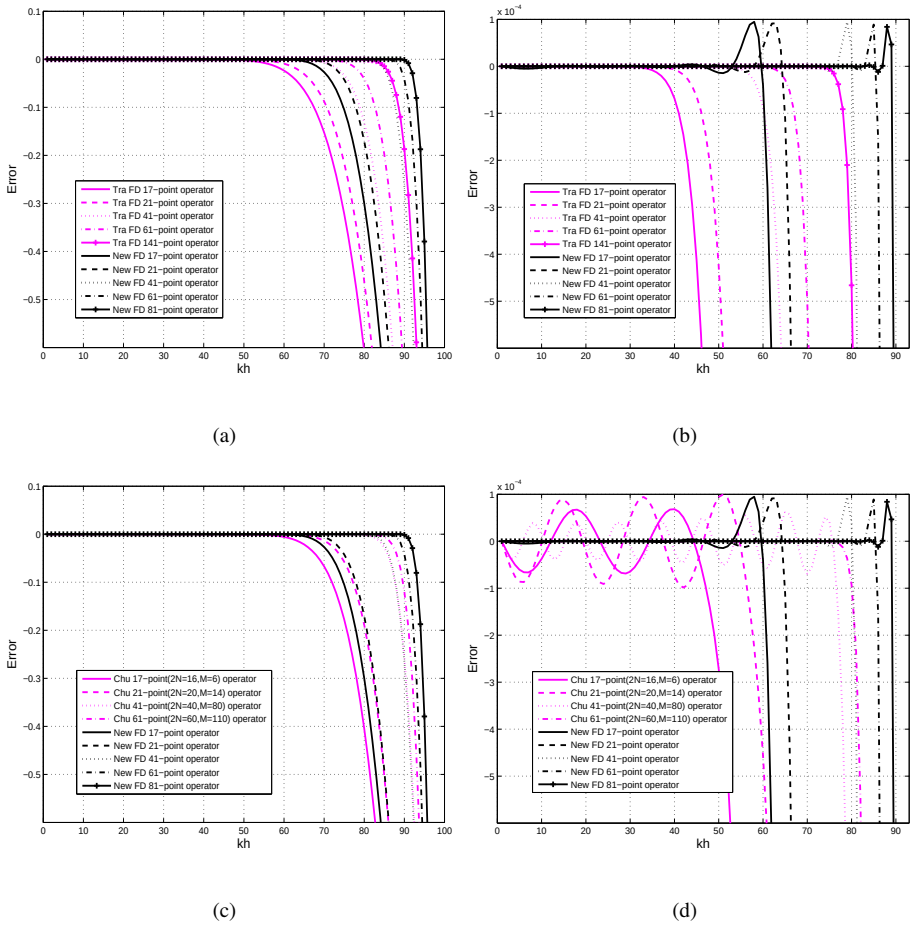

Figure 1: (a) Comparison of dispersion errors of the FD operator for the first derivative using the traditional method and the new method; (b) locally zoomed illustration of the dispersion errors of the FD operator for the first derivative using the traditional method and the new method; (c) Comparison of dispersion errors of the FD operator for the first derivative using the method of (Chu and Stoffa, 2012) and the new method; (d) locally zoomed illustration of the dispersion errors of the FD operator for the first derivative using the method of (Chu and Stoffa, 2012) and the new method. In this figure, the horizontal axis refers to the percentage of kh range.

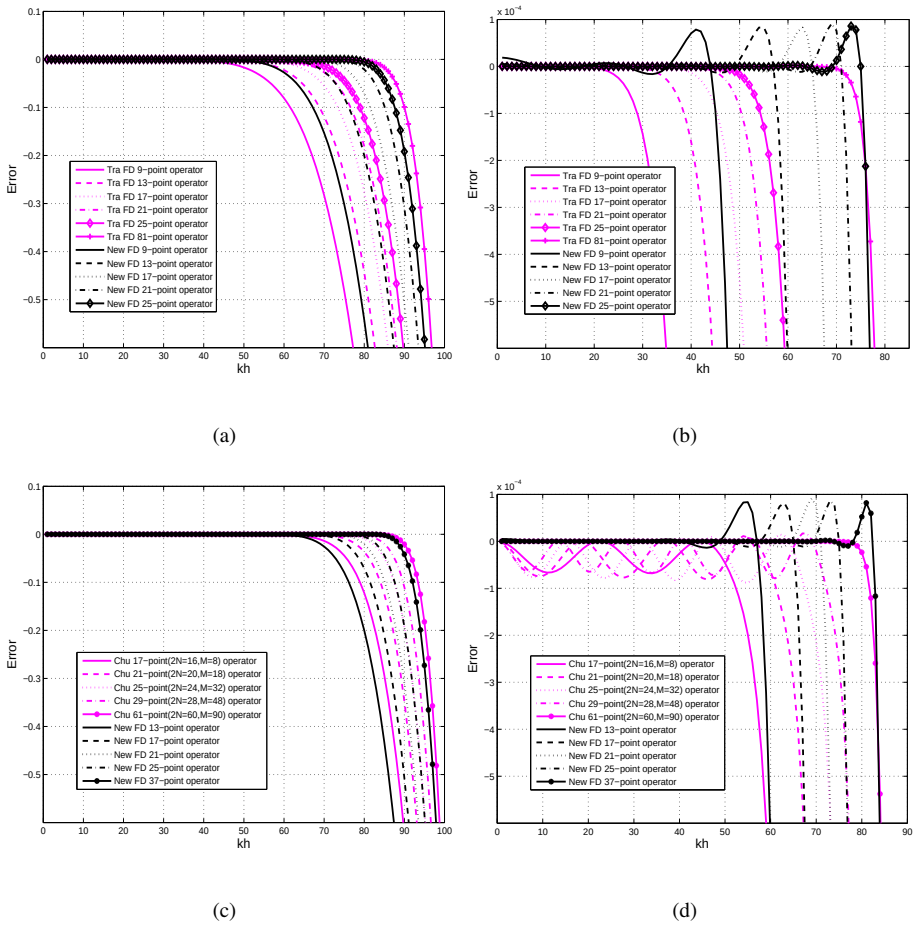

Figure 2: (a) Comparison of dispersion errors of the FD operator for the second derivative using the traditional method and the new method; (b) locally zoomed illustration of the dispersion errors of the FD operator for the second derivative using the traditional method and the new method; (c) Comparison of dispersion errors of the FD operator for the second derivative using the method of (Chu and Stoffa, 2012) and the new method; (d) locally zoomed illustration of the dispersion errors of the FD operator for the second derivative using the method of (Chu and Stoffa, 2012) and the new method. In this figure, the horizontal axis refers to the percentage of kh range.

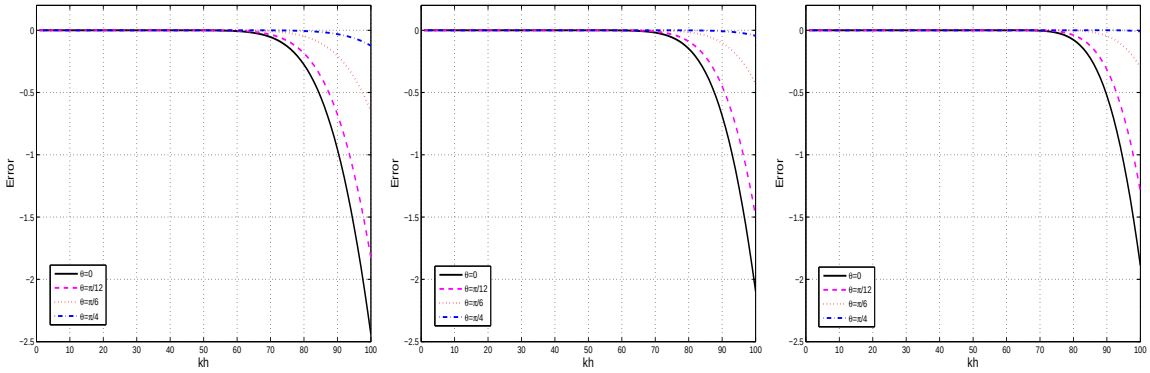

(a) (b) (c)

Figure 3: (a) Dispersion errors of the traditional FD operator for 2D wave equation; (b) dispersion errors of the optimized binomial windowed FD operator for 2D wave equation; (c) dispersion errors of the new dispersion-relationship-preserving FD operator for 2D wave equation. In this figure, the horizontal axis refers to the percentage of kh range.

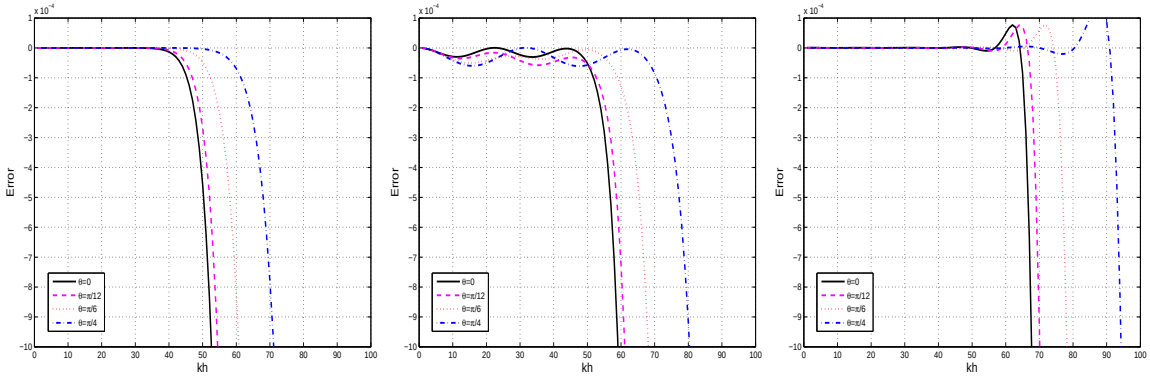

(a) (b) (c)

Figure 4: (a) Locally zoomed illustration of the dispersion errors of the traditional FD operator for 2D wave equation; (b) locally zoomed illustration of the dispersion errors of the optimized binomial windowed FD operator for 2D wave equation; (c) locally zoomed illustration of the dispersion errors of the new dispersion-relationship-preserving FD operator for 2D wave equation. In this figure, the horizontal axis refers to the percentage of kh range.

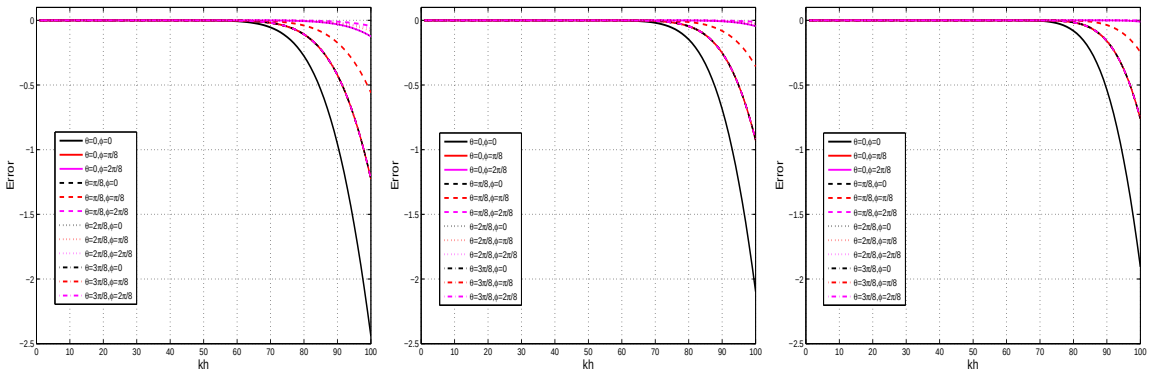

(a) (b) (c)

Figure 5: (a) Dispersion errors of the traditional FD operator for 3D wave equation; (b) dispersion errors of the optimized binomial windowed FD operator for 3D wave equation; (c) dispersion errors of the new dispersion-relationship-preserving FD operator for 3D wave equation. In this figure, the horizontal axis refers to the percentage of kh range.

Finally, we measure the dispersion errors of the 3D FD operator for the second derivative using the following formula:

$$E_3 = -3c_0 - 2\sum_{m=1}^{N} c_m(\cos(mkh\cos\theta\cos\phi) + \cos(mkh\cos\theta\sin\phi) + \cos(mkh\sin\theta)) - k^2h^2. \qquad (23)$$

The smaller value of E_3, the less dispersion of the 3D FD operator will be.

Dispersion errors of the FD operator when $N = 8$ for different methods are shown in Figure 5. To clearly show the dispersion effect, we zoomed Figures 5(a)-5(c) to Figures 6(a)-6(c), respectively. It reveals that for a dispersion error between -1.0×10^{-4} and 1.0×10^{-4}, the traditional method covers 45% of the kh range, the binomial windowed method covers 52% of the kh range, whereas the new dispersion-relationship-preserving method can extend to 65% of the kh range. Hence the new method could preserve dispersion relation within a larger interval of frequencies and angles. The results agree with the 1D and 2D cases.

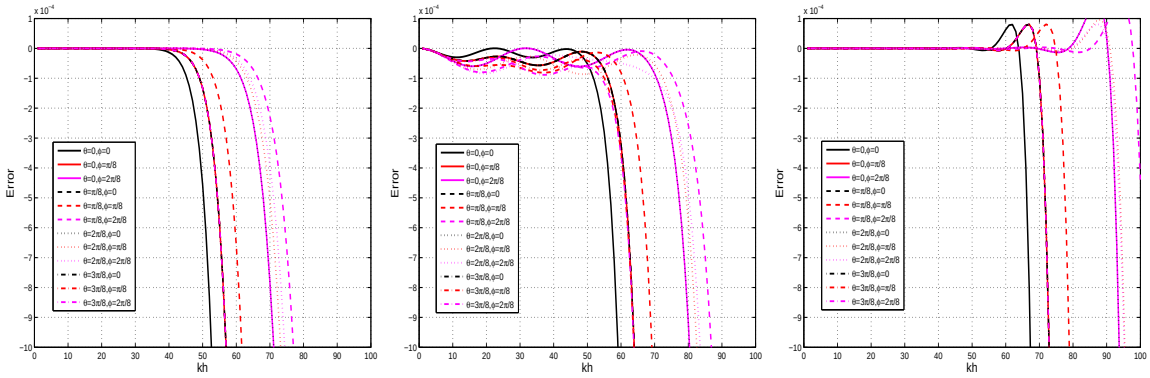

(a) (b) (c)

Figure 6: (a) Locally zoomed illustration of the dispersion errors of the traditional FD operator for 3D wave equation; (b) locally zoomed illustration of the dispersion errors of the optimized binomial windowed FD operator for 3D wave equation; (c) locally zoomed illustration of the dispersion errors of the new dispersion-relationship-preserving FD operator for 3D wave equation. In this figure, the horizontal axis refers to the percentage of kh range.

5 Numerical simulations

5.1 A simple model

We first consider a simple isotropic model with velocity equaling 2000m/s, spatial sampling interval equaling 20m, temporal step of 1ms and $N = 8$ for all FD operators. The source is located in the center of the test area. The source wavelet is the second derivative of the Gaussian function defined as

$$w(t) = 10^6 \exp(-f_0^2(t-t_0)^2), \tag{24}$$

where the frequency f_0 is 55Hz, and t_0 is the time zero delay chosen as $4/f_0$.

To show differences of the snapshots of the traditional method, the optimized binomial windowed method ($2N = 16$, $M = 16$) and the new dispersion-relationship-preserving method ($r = 0.8$, f is assumed to be 40 Hz in equation (8)) at the time equaling 1000ms, we plot slices of the snapshots of the wavefield in Figure 7(a)-7(c). The comparison reveals that both the optimized binomial windowed method and the new dispersion-relationship-preserving method can reduce the dispersion, whereas the later can reduce it more, and hence

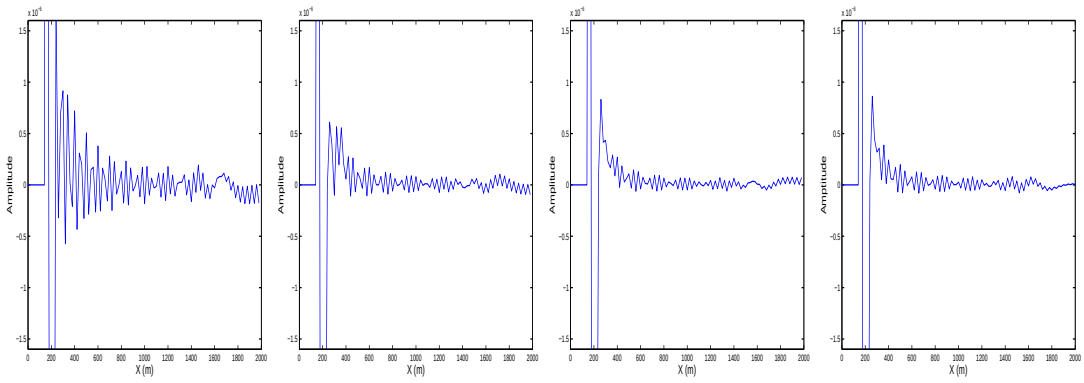

(a) (b) (c) (d)

Figure 7: (a) Slice of snapshot of the wavefield with the traditional method; (b) Slice of snapshot of the wavefield with the optimized binomial windowed method; (c) Slice of snapshot of the wavefield with the new dispersion-relationship-preserving method; (d) Slice of snapshot of the wavefield with the least squares method.

providing a more accurate wavefield simulation. To demonstrate the performance of the proposed method, we add a slice in Figure 7(d) by using the well-known least squares method (see e.g., (Atle, 2011)). For this method, when $r = 0.72$ it maintains the 1/10000 error limitation, whereas for $r = 0.8$, it maintains the 1/1000 error limitation. It is obvious that the performance of proposed method is close to the least squares method. However, the proposed method needs much less time/effort to get the FD coefficients.

5.2 Salt model

In the following, we present simulation results using a widely referred salt velocity model from the Society of Exploration of Geophysics. The velocity model is shown in Figure 8 with variations of velocities from 1500m/s to 4800m/s, spatial sampling interval equaling 20m, temporal step of 1ms and $N = 7$ for all FD operators. The same source function as in former examples is applied with $f_0 = 45$Hz. We take f in equation (8) as 28Hz. When the velocity is 1486m/s, r equals 0.7537; while when the velocity is 4870m/s, r equals 0.23. The simulation results using the traditional finite difference method, the optimized binomial windowed method and the new dispersion-relationship-preserving method are displayed in Figures 9(a)-9(c), respectively. To show details of their difference, we plot slices of the seismic records in Figures 10(a)-10(c). We also plot

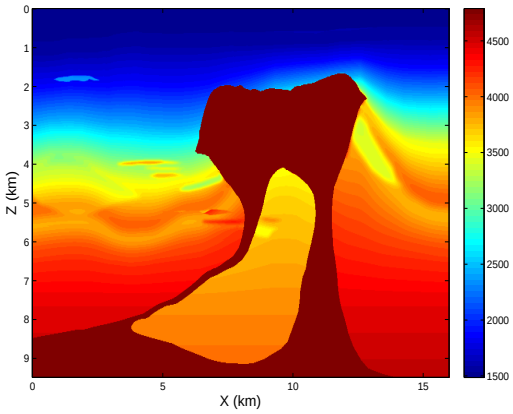

Figure 8: Salt velocity model

the seismic records at 13km for all methods together in Figure 11. It is evident that the new method provides the better simulation results with least dispersion than others.

6 Conclusion

We have developed a new method for determining the FD coefficients. The new aspects of the method are: (1) the method specifies a upper limit of the wavenumber (frequency) according to the maximum of the source frequency, the spatial grid interval and the velocity; (2) assumption is made on N uniformly distributed grid nodes satisfying the dispersion property within the wavenumber (frequency) domain; (3) FD coefficients are solved through a well-conditioned linear system.

With the dispersion analysis of our new method, and the comparison with the traditional FD coefficients determination method, the optimized binomial windowed FD coefficients determination method and the least squares method, we conclude that our method is superior to previous methods and is comparable to the least square method while the new method is much easy/efficient to get the FD coefficients. As a result, our method can be a substitute to the spatial Taylor expansion methods and can be applied in forward seismic wave modeling and reverse time migration.

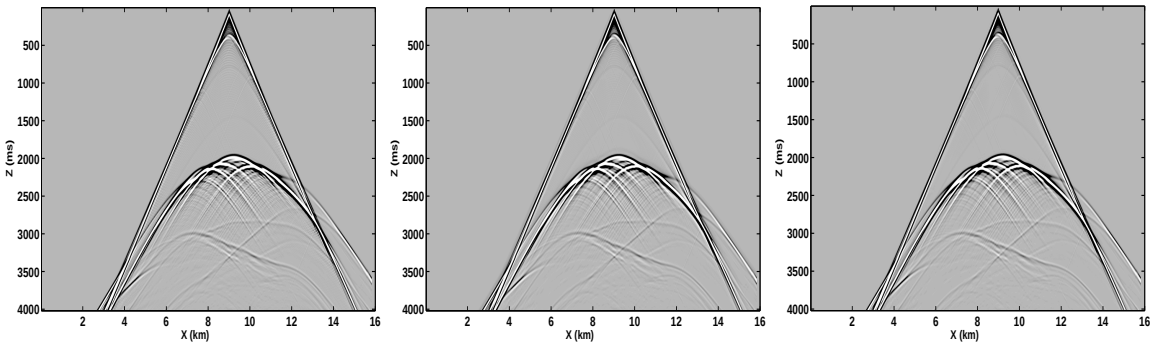

(a) (b) (c)

Figure 9: (a) Seismic records of the salt model with the traditional method; (b) seismic records of the salt model with the binomial windowed method; (c) seismic records of the salt model with the new dispersion-relationship-preserving method.

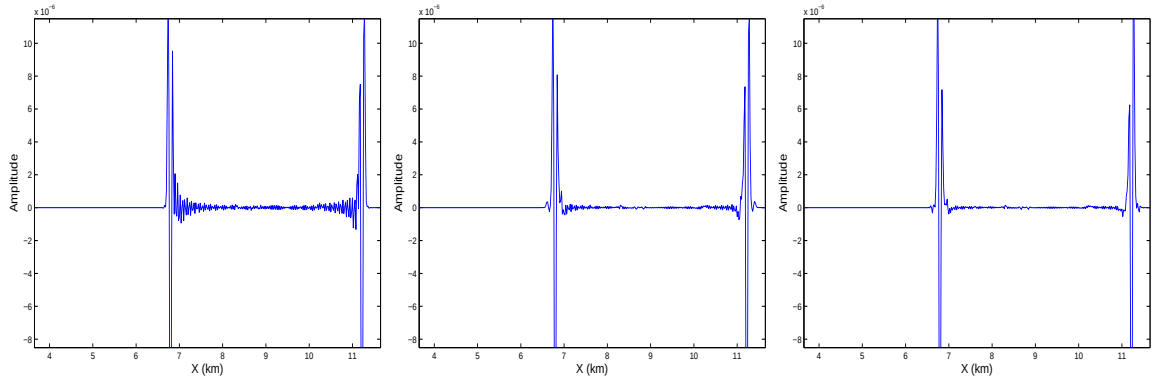

(a) (b) (c)

Figure 10: (a) Slice of seismic records of the salt model with the traditional method; (b) slice of seismic records of the salt model with the binomial windowed method; (c) slice of seismic records of the salt model with the new dispersion-relationship-preserving method.

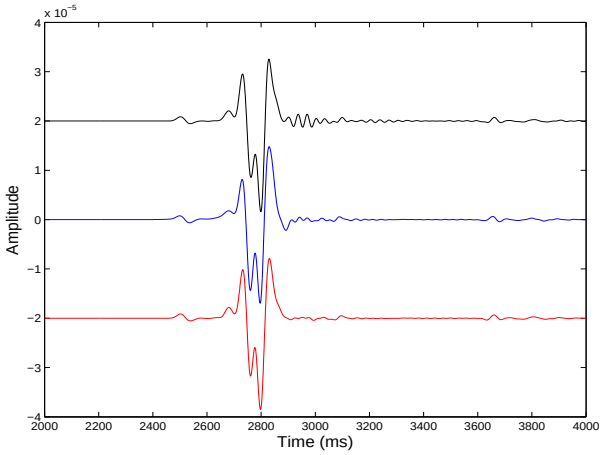

Figure 11: From the top to the bottom are slices of seismic records from Figure 9(a) to (c), respectively. These seismic records are recorded at 13km.

Acknowledgements

We deeply acknowledge the associate editor's constructive review that improved the manuscript. We are grateful to anonymous reviewers for their very helpful comments on improvement of our paper. We are also quite thankful to Prof. Zuhair Nashed for his suggestions and technical discussions. This work is supported by National Natural Science Foundation of China under grant numbers 11271349, 41325016 and R & D of Key Instruments and Technologies for Deep Resources Prospecting (the National R & D Projects for Key Scientific Instruments) under grant number ZDYZ2012-1-02-04.

References

Abdelkhalek R., Calandra H., Coulaud O., Latu G. and Roman J. 2012. Fast seismic modeling and reverse time migration on a graphics processing unit cluster. *Geophysical Prospecting* **24**, 739-750.

Atle A. 2011. TTI finite difference with variable grid in depth. *SEG Technical Program Expanded Abstracts*, 2011 SEG Annual Meeting, September 18-23, San Antonio, Texas.

Bansal R. and Sen M. K. 2008. Finite-difference modelling of S-wave splitting in anisotropic media. *Geophysical Prospecting* **56**, 293-312.

Buur J. and Kuhnel T. 2008. Salt interpretation enabled by reverse-time migration. *Geophysics* **73**(5), VE211-VE216.

Chu C. and Stoffa P. L. 2012. Determination of finite-difference weights using scaled binomial windows. *Geophysics* **77**(3), W17-W26.

Dablain M. A. 1986. The application of high-order differencing to the scalar wave equation. *Geophysics* **51**(1), 54-66.

Etgen J. T. and O'Brien M. J. 2007. Computational methods for large-scale 3D acoustic finite-difference modeling: A tutorial. *Geophysics* **72**(5), SM223-SM230.

Fornberg B. 1987. The pseudospectral method: Comparisons with finite differences for the elastic wave equation. *Geophysics* **52**(4), 483-501.

Guan H., Dussaud E., Denel B. and Williamson P. 2011. Techniques for an efficient implementation of RTM in TTI media, SEG Technical Program Expanded Abstracts, 3393-3397.

Kelly K. R., Ward R. W., Treitel S. and Alford R. M. 1976. Synthetic seismograms: a finite-difference approach, *Geophysics* **41**, 2-27.

Liu H. W., Li B., Liu H., Tong X. L., Liu Q., Wang X. W. and Liu W. Q. 2012. The issues of prestack reverse time migration and solutions with Graphic Processing Unit implementation. *Geophysical Prospecting* **60**(5), 906-918.

McMechan G. A. 1989. A review of seismic acoustic imaging by reverse-time migration. *Geophysical Prospecting* **1**, 18-21.

Virieux J., Calandra H. and Plessix R. 2011. A review of the spectral, pseudo-spectral, finite-difference and finite-element modelling techniques for geophysical imaging. *Geophysical Prospecting* **59**, 794-813.

Yang D. H., Tong P. and Deng X. Y. 2012. A central difference method with low numerical dispersion for solving the scalar wave equation. *Geophysical Prospecting* **60**, 885-905.

Ye F. and Chu C. 2005. Dispersion-relation-preserving finite difference operators: derivation and application. SEG Technical Program Expanded Abstracts, 1783-1786.

Zhang Y., Zhang H. Z. and Zhang G. Q. 2011. A stable TTI reverse time migration and its implementation. *Geophysics* **76**(3), WA3-WA11.